Semiclassical Assignment of the Vibrational Spectrum of N2O

Waalkens, Holger; Jung, Christof; Taylor, Howard S.

Published in:
The Journal of Physical Chemistry. A: Molecules, Spectroscopy, Kinetics, Environment, & General Theory

Publication date:
2002

Semiclassical Assignment of the Vibrational Spectrum of N_2O

Holger Waalkens*

Institut für Theoretische Physik and Institut für Dynamische Systeme, Universität Bremen, Postfach 330 440, 28334 Bremen, Germany

Christof Jung

Centro de Ciencias Fisicas UNAM, Apdo. postal 48-3, 62551 Cuernavaca, Mexico

Howard S. Taylor

Department of Chemistry, University of Southern California, Los Angeles, California 90089

Received: August 7, 2001; In Final Form: November 13, 2001

The vibrational spectrum of N_2O as given by an effective spectroscopic Hamiltonian based on the existence of a superpolyad number is analyzed and assigned in terms of classical motions. The effective Hamiltonian includes a large number of resonances of which only one is dominant for low and intermediate superpolyad numbers. In this energy range, the corresponding classical system is quasi-integrable and can be described in terms of a system with only one nontrivial degree of freedom. This integrable system can be analyzed by considering the so-called "quantizing trajectories" on a "polyad sphere". This method is no longer applicable when the superpolyad number is further increased and classical chaos comes into play. We then turn to a powerful universal method based on the graphical representation of semiclassical wave functions on a naturally appearing toroidal configuration space. These wave functions are obtained using the already known transformation matrix used in fitting the effective Hamiltonian. Experience with the interpretation of the resulting figures allows one to draw conclusions on the classical internal motions and therefore on the assignment of the quantum states without any further calculation. As such, the method is of particular interest to nontheorists and to nonspecialists in the fields of nonlinear dynamics and quantum calculation. For higher superpolyad numbers, the chaos remains mainly concentrated about the direct neighborhood of a separatrix of the former integrable system so that a great part of the vibrational spectrum can still be assigned in terms of the EBK quantum numbers of quantized tori.

1. Introduction

Following experiments on carbon dioxide,[1] Teffo, Perevalov, and Lyulin introduced a spectroscopic Hamiltonian for nitrous oxide[2] based on the approximate relations between harmonic frequencies

$$\omega_1/\omega_2 \approx 2{:}1, \quad \omega_2/\omega_3 \approx 1{:}4 \tag{1}$$

where ω_1, ω_2, and ω_3 refer to the harmonic frequencies of the symmetric stretch, the bend, and the asymmetric stretch, respectively. The quality of the spectroscopic Hamiltonian, which incorporates a large number of resonances, was confirmed by a combination of high-resolution Fourier transform spectroscopy and intracavity laser absorption spectroscopy between 6500 and 11 000 cm^{-1} and between 11 700 and 15 000 cm^{-1}, respectively.[3] From a general point of view of physics and chemistry, the fit of a quantum spectrum to a spectroscopic Hamiltonian cannot be the final step in the analysis of a vibrational spectrum. In addition the question of the relation of the spectra to the underlying classical motion has to be answered. The answer to this question is not only necessary for the assignment of the quantum states but of further importance because it contains, for example, information needed to understand isomerization and reactivity.

In this paper, we are concerned with the assignment of the pure vibrational spectrum of N_2O. The first step toward an assignment is already given through the existence of a superpolyad number,[4] which is directly connected to the resonances in eq 1 and of which the conservation was the basis for the construction of the spectroscopic Hamiltonian. One can proceed with the assignment by looking at the corresponding classical system. The spectroscopic Hamiltonian as given in the number representation can be translated to classical mechanics via the standard application of Heisenberg's correspondence principle. The result is a classical Hamiltonian given in action angle variables (I_i, ϕ_i). The appearance of action angle variables underlies the idea that originally there exists a classically integrable system derived from the quantum Hamiltonian without off-diagonal elements for which the inclusion of the off-diagonal elements acts as a perturbation. For an integrable system, the Liouville−Arnold theorem[5] says that phase space is generically foliated by invariant tori. Here, action angle variables are the most suitable coordinates with the angles parametrizing the tori for fixed actions. Accordingly, Hamilton's equations of motion assume the simple form

* To whom correspondence should be addressed. Phone: +49 421 218-4566. Fax: +49 421 218-4869. E-mail: waalkens@physik.uni-bremen.de.

10.1021/jp013057w CCC: $22.00
Published on Web 01/18/2002

$$\dot{I}_i = -\frac{\partial \mathcal{H}}{\partial \phi_i} = 0, \quad \dot{\phi}_i = \frac{\partial \mathcal{H}}{\partial I_i} \equiv \omega_i \tag{2}$$

that is, the actions are constants of the motion and the angles, ϕ_i, increase in time with constant frequencies, ω_i. Action angle variables are, for example, essential for the discussion of how an integrable system reacts to a small perturbation. In such a case, KAM theory guarantees the survival of tori with sufficiently irrational frequency ratios. For the classical analogue of the quantum mechanical molecule with vibrational degrees of freedom, the integrability-destroying perturbation appears quantum mechanically through the inclusion of off-diagonal elements. This perturbation is, in general, not small. Nevertheless, the action angle variables of the unperturbed system are quite useful even for the description of a perturbed system, which usually exhibits significant features of chaos. This is especially valid in molecular physics in which the energies reached before the dissociation of the molecule are often high enough to destroy most of the original tori and to produce a complex phase space with a number of resonance zones[6] but which fortunately are not high enough to destroy all regular structures in phase space. Furthermore, very small structures, which might exist in phase space, are not visible in quantum mechanics because of a nonvanishing Planck's constant, and in this way, quantum mechanics seems to average over the classical motions. Therefore, a great number of the quantum states of a vibrational molecule are roughly localized on more or less pronounced KAM tori or the tori that surround stable periodic orbits, which are the centers of the resonance zones and which are characterized by a phase lock of the angle variables. This offers the opportunity to associate whole series of quantum states with KAM primary tori or periodic orbits and to assign them by quantum numbers of EBK type.

The common procedures of the classical analysis remain feasible for systems with up to two effective degrees of freedom in which the four-dimensional phase space can still be analyzed in terms of two-dimensional Poincaré surfaces of section. For systems in molecular physics with a superpolyad number, there exists the opportunity to separate off explicitly the trivial degree of freedom connected to the superpolyad number. The corresponding separating coordinates are some linear combination of the angle variables. Although this separability is taken advantage of in many works in this field as far as the classical analysis is concerned,[7] the separability is utilized for the quantum mechanics only in rare exceptions.[8] A classification of the quantum states is usually attempted through the representation of wave functions in the original Cartesian type of coordinates, which may be either normal- or local-mode coordinates. The fact that there is still hidden a trivial degree of freedom in these coordinates because they do not allow for a separation makes it difficult to find a classification scheme. Instead, it is ultimately simpler to carry out the analysis in the reduced dimension space of the separated angle variables even for the quantum mechanical analysis. A representation of the quantum states with respect to these angles can be easily obtained with no new calculation. This representation is only meaningful in a semiclassical sense but is totally sufficient for the purpose of an assignment and the analysis of the classical motions. The result is a wave function on a two-dimensional toroidal configuration space, which is easy to present graphically in terms of density plots and plots of the phases of the wave functions. The density plots serve for the identification of the underlying classical motion and for the sorting of the states in a polyad into ladders of levels, each based on a unique classical motion. Quantum numbers are obtained from either counting nodal lines in the density plots or counting phase advances in the phase plots. The simplicity of this method on one hand and its great power on the other hand were already demonstrated via the application to the complex vibrational spectra of acetylene[9,10] and CHBrClF.[11] The method is especially useful for those who are not specialists in the fields of nonlinear dynamics and quantum calculations because, as mentioned above, the representation needs no serious calculation. The only hurdle that remains is the ability to mentally and visually work with action angle variables, which at first are rather abstract variables. Once done, there is no difficulty to lift the motion described with respect to action angle variables back to the corresponding motion with respect to the original Cartesian type of coordinates. This is made possible by the observation that, although the formal relation of the action angle variables to the original Cartesian type of coordinates generally may be very complicated, it usually is a very good approximation to lift the action angle variables back to the Cartesian type of coordinates as if they were related via a first-order canonical perturbation theory.[12−14]

Our analysis of N_2O is mainly divided into two parts. For low and intermediate superpolyad numbers, a resonance between the symmetric stretch and the bend is so dominant that other resonances are of minor importance and can be neglected. The quantum number corresponding to the asymmetric stretch remains a second good quantum number along with the superpolyad number. In this case, it is appropriate to replace the superpolyad number by a linear combination of only those quantum numbers that are no longer good quantum numbers.[7] To distinguish it from the superpoyad number, this quantum number will be referred to as the polyad number. Classically, the asymmetric stretch can be approximately separated off, and there remains an integrable system with only one effective degree of freedom. The phase space of the one degree of freedom system has the topology of a sphere. The dynamics on this so-called "polyad sphere" is discussed, and it is related to the quantum system through the representation of so-called "quantizing trajectories", which are the projections of the quantized tori onto this sphere. This is the subject of the first part in which we particularly concentrate on superpolyad 14 of which 8 of its 20 bands could be measured by Campargue et al.[3] In the second part, the superpolyad number is further increased and the other resonances become important. The asymmetric stretch can no longer be separated off, and the classical dynamics becomes chaotic. A polyad sphere no longer exists, and an analysis as in the first part is no longer possible. We then switch to our procedure mentioned above and illustrate it for the eigenstates of superpolyad 22 of which 2 of its 42 bands could be measured Campargue et al.[3] Alternatively, it will be seen that from the relations of the two remaining angles of the reduced dimension toroidal configuration space to the three original angles and from the visually recognizable location of the wave function density on the 2 torus most conclusions about the motion in original molecular coordinates can be inferred without further calculation. Moreover, this analysis is also applicable to the one-resonance case. This all means that the classification of states can be effectively done without using nonlinear classical analysis. The outline of this paper is as follows. In section 2, the classical Hamiltonian is derived from applying Heisenberg's correspondence principle to the spectroscopic Hamiltonian, which is explicitely represented in terms of creation and annihilation operators. In section 3, N_2O is analyzed by incorporating exclusively the dominating Fermi resonance between the symmetric stretch and the bend. The

energy regime in which chaos comes into play and the analysis based on the presentation of semiclassical wave functions on the torus of the angle variables is the subject of section 4. Concluding remarks and an outlook are given in section 5.

2. Quantum and Classical Hamiltonian

To derive the classical analogue to the effective quantum Hamiltonian presented by its matrix elements by Teffo, Perevalov, and Lyulin,[2] we write the effective Hamiltonian explicitly in terms of creation and annihilation operators. It can be divided into three terms,

$$\hat{H} = \hat{H}_0^{\text{lin}} + \hat{H}_0^{\text{anh}} + \hat{H}_1 \tag{3}$$

where $\hat{H}_0^{\text{lin}}$ is the harmonic term, $\hat{H}_0^{\text{anh}}$ is the nonharmonic part of the Dunham expansion, and $\hat{H}_1$ includes all of the off-diagonal terms. To write the terms explicitly, we introduce the abbreviations

$$\hat{I}_1 \equiv \frac{1}{2}(\hat{a}_1^\dagger \hat{a}_1 + \hat{a}_1 \hat{a}_1^\dagger) \tag{4}$$

$$\hat{I}_2 \equiv \frac{1}{2}(\hat{a}_{2d}^\dagger \hat{a}_{2d} + \hat{a}_{2d} \hat{a}_{2d}^\dagger + \hat{a}_{2g}^\dagger \hat{a}_{2g} + \hat{a}_{2g} \hat{a}_{2g}^\dagger) \tag{5}$$

$$\hat{I}_3 \equiv \frac{1}{2}(\hat{a}_3^\dagger \hat{a}_3 + \hat{a}_3 \hat{a}_3^\dagger) \tag{6}$$

where $\hat{a}_{2d/g}^\dagger$ and $\hat{a}_{2d/g}$ are the creation and annihilation operators for the degenerate bend degrees of freedom with d and g referring to droit (right) and gauche (left) in the notation of Cohen-Tannoudji, Diu, and Laloë.[15] The linear term and the second- and third-order anharmonic term then read

$$\hat{H}_0^{\text{lin}} = \omega_1 \hat{I}_1 + \omega_2 \hat{I}_2 + \omega_3 \hat{I}_3 \tag{7}$$

$$\begin{aligned}\hat{H}_0^{\text{anh}} = {} & x_{11}\hat{I}_{12} + x_{12}\hat{I}_1\hat{I}_2 + x_{13}\hat{I}_1\hat{I}_3 + x_{22}\hat{I}_2{}^2 + x_{23}\hat{I}_2\hat{I}_3 + \\ & x_{33}\hat{I}_3{}^2 + y_{111}\hat{I}_1{}^3 + y_{112}\hat{I}_1{}^2\hat{I}_2 + y_{123}\hat{I}_1\hat{I}_2\hat{I}_3 + y_{113}\hat{I}_1{}^2\hat{I}_3 + \\ & y_{122}\hat{I}_1\hat{I}_2{}^2 + y_{133}\hat{I}_1\hat{I}_3{}^2 + y_{222}\hat{I}_2{}^3 + y_{223}\hat{I}_2{}^2\hat{I}_3 + y_{233}\hat{I}_2\hat{I}_3{}^2 + \\ & y_{333}\hat{I}_3{}^3\end{aligned} \tag{8}$$

The term H_1 is the sum of a 1:2 Fermi resonance for the symmetric stretch and the bend

$$\begin{aligned}\hat{H}_{1s:2b} = {} & F_e^{(2)}2(\hat{a}_1^\dagger \hat{a}_{2d} \hat{a}_{2g} + \text{adj}) + F_1^{(2)}2(\hat{a}_1^\dagger \hat{a}_1 \hat{a}_1^\dagger \hat{a}_{2d} \hat{a}_{2g} + \text{adj}) + \\ & F_2^{(2)}2(\hat{a}_1^\dagger \hat{a}_{2d} \hat{a}_{2g} \hat{a}_{2g}^\dagger \hat{a}_{2g} + \hat{a}_1^\dagger \hat{a}_{2d} \hat{a}_{2d}^\dagger \hat{a}_{2d} \hat{a}_{2g} + \text{adj}) + \\ & F_3^{(2)}2(\hat{a}_1^\dagger \hat{a}_{2d} \hat{a}_{2g} \hat{I}_3 + \text{adj})\end{aligned} \tag{9}$$

a 2:1 Fermi resonance for the symmetric stretch and the asymmetric stretch

$$\begin{aligned}\hat{H}_{2s:1a} = {} & F_e^{(3)}(\hat{a}_1^\dagger \hat{a}_1^\dagger \hat{a}_3 + \text{adj}) + F_1^{(3)}(\hat{a}_1^\dagger \hat{I}_1 \hat{a}_1^\dagger a_3 + \text{adj}) + F_2^{(3)} \\ & (\hat{a}_1^\dagger \hat{a}_1^\dagger a_3 \hat{I}_2 + \text{adj}) + F_3^{(3)}(\hat{a}_3 \hat{a}_3^\dagger \hat{a}_3 \hat{a}_1^\dagger \hat{a}_1^\dagger + \text{adj})\end{aligned} \tag{10}$$

a Fermi resonance involving a three-mode interaction

$$\begin{aligned}\hat{H}_{1s:2b:1a} = {} & F_e^{(4)}2(\hat{a}_1^\dagger \hat{a}_{2d}^\dagger \hat{a}_{2g}^\dagger \hat{a}_3 + \text{adj}) + F_1^{(4)}2(\hat{a}_1^\dagger \hat{a}_1 \hat{a}_1^\dagger \hat{a}_{2d}^\dagger \hat{a}_{2g}^\dagger \hat{a}_3 + \\ & \text{adj}) + F_2^{(4)}2(\hat{a}_{2g}^\dagger \hat{a}_{2g} \hat{a}_{2g}^\dagger \hat{a}_{2d}^\dagger \hat{a}_1^\dagger \hat{a}_3 + \hat{a}_{2d}^\dagger \hat{a}_{2d} \hat{a}_{2d}^\dagger \hat{a}_{2g}^\dagger \hat{a}_1^\dagger \hat{a}_3 + \text{adj}) + \\ & F_3^{(4)}2(\hat{a}_3 \hat{a}_3^\dagger \hat{a}_3 \hat{a}_1^\dagger \hat{a}_{2g} \hat{a}_{2d} + \text{adj})\end{aligned} \tag{11}$$

plus higher-order terms

$$F^{(10)}4(\hat{a}_3 \hat{a}_{2d}^\dagger \hat{a}_{2d}^\dagger \hat{a}_{2g}^\dagger \hat{a}_{2g}^\dagger + \text{adj}) + \tag{12}$$

$$F^{(11)}4(\hat{a}_1^\dagger \hat{a}_1^\dagger \hat{a}_{2d} \hat{a}_{2d} \hat{a}_{2g} \hat{a}_{2g} + \text{adj}) + \tag{13}$$

$$F^{(12)}(\hat{a}_1^\dagger \hat{a}_1^\dagger \hat{a}_1^\dagger \hat{a}_1^\dagger \hat{a}_3 \hat{a}_3 + \text{adj}) + \tag{14}$$

$$F^{(13)}2(\hat{a}_1^\dagger \hat{a}_1^\dagger \hat{a}_1^\dagger \hat{a}_{2d} \hat{a}_{2g} \hat{a}_3 + \text{adj}) \tag{15}$$

In the expressions above, the creation and annihilation operators appear symmetrically for each degree of freedom. A classical Hamiltonian can therefore be obtained directly from Heisenberg's correspondence principle

$$\hat{a}_i^\dagger \rightarrow \sqrt{I_i}\exp(i\phi_i), \quad \hat{a}_i \rightarrow \sqrt{I_i}\exp(-i\phi_i) \tag{16}$$

where I_i and ϕ_i are the canonical action angle variables of the corresponding classical system. The creation and annihilation operators, $\hat{a}_{2d/g}^\dagger$ and $\hat{a}_{2d/g}$, only appear in such a way that they conserve the total number of quanta in the degenerate bend degrees of freedom, 2d and 2g. This is necessary to secure a vanishing vibrational angular momentum. It is therefore convenient to introduce the classical action $I_2 \equiv I_{2d} + I_{2g}$ of which the classical interpretation is the radial action of a two-dimensional isotropic oscillator separated in polar coordinates. The expressions for $\mathscr{H}_0^{\text{lin}}$ and $\mathscr{H}_0^{\text{anh}}$ are immediately obtained from replacing in eqs 7 and 8 the operators $\hat{I}_i$ by the classical actions I_i. For the interaction term one finds

$$\begin{aligned}\mathscr{H}_1 = {} & 2(F_e^{(2)}\sqrt{I_1}I_2 + F_1^{(2)}I_1{}^{3/2}I_2 + F_2^{(2)}\sqrt{I_1}I_2{}^2 + \\ & F_3^{(2)}\sqrt{I_1}I_2I_3)\cos(\phi_1 - 2\phi_2) + 2(F_e^{(3)}I_1\sqrt{I_3} + F_1^{(3)}I_1{}^2\sqrt{I_3} + \\ & F_2^{(3)}I_1\sqrt{I_3}I_2 + F_3^{(3)}I_1I_3{}^{3/2})\cos(2\phi_1 - \phi_3) + 2(F_e^{(4)}\sqrt{I_1}I_2\sqrt{I_3} + \\ & F_1^{(4)}I_1{}^{3/2}I_2\sqrt{I_3} + F_2^{(4)}\sqrt{I_1}I_2{}^2\sqrt{I_3} + F_3^{(4)}\sqrt{I_1}I_2I_3{}^{3/2})\cos(\phi_1 + \\ & 2\phi_2 - \phi_3) + 2F^{(10)}I_2{}^2\sqrt{I_3}\cos(4\phi_2 - \phi_3) + \\ & 2F^{(11)}I_1I_2{}^2\cos(2\phi_1 - 4\phi_2) + 2F^{(12)}I_1{}^2I_3\cos(4\phi_1 - 2\phi_3) + \\ & 2F^{(13)}I_1{}^{3/2}I_2\sqrt{I_3}\cos(3\phi_1 - 2\phi_2 - \phi_3)\end{aligned} \tag{17}$$

The appearance of action angle variables underlies the idea that we originally had a classically integrable system described by the Hamiltonian $\mathscr{H}_0 = \mathscr{H}_0^{\text{lin}} + \mathscr{H}_0^{\text{anh}}$, which only depends on the action variables to which a perturbation $\mathscr{H}_1$ is added, which explicitly depends on the angles so that the actions are in general no longer constants of the motion. The resonances, $n_1^{(i)}\phi_1 + n_2^{(i)}\phi_2 + n_3^{(i)}\phi_3$ with $(n_1^{(i)}, n_2^{(i)}, n_3^{(i)}) \in Z^3$, in the argument of the cosine functions are linear combinations of the two approximate resonance conditions, $\langle n,\omega \rangle = 0$ with $n = (1,-2,0)$ and $\langle m,\omega \rangle = 0$ with $m = (0,4,-1)$, given by eq 1. Because a perturbation $f^{(i)}(I_1,I_2,I_3)\cos(n_1^{(i)}\phi_1 + n_2^{(i)}\phi_2 + n_3^{(i)}\phi_3)$ is constant on a hyperplane $n_1^{(i)}\phi_1 + n_2^{(i)}\phi_2 + n_3^{(i)}\phi_3 = 0$ in the three-dimensional space of the angles (ϕ_1,ϕ_2,ϕ_3), the hyperplane is not affected by the perturbation. The actions corresponding to the angles, which span that hyperplane, would remain being constants of the motion. Because the perturbation $\mathscr{H}_1$ consists of a mixture of the two linearly independent resonances **n** and **m**, there remains only a single line in angle space that is invariant under the perturbation. The direction of this line is $\mathbf{n} \times \mathbf{m} = (2,1,4)$. Let us derive a canonical transform from the old angles $\boldsymbol{\phi} = (\phi_1,\phi_2,\phi_3)$ and actions $\mathbf{I} = (I_1,I_2,I_3)$ to new angles $\boldsymbol{\psi} = (\psi_1,\psi_2,\psi_3)$ and actions $\mathbf{J} = (J_1,J_2,J_3)$ so that ψ_1 points in the invariant direction $\mathbf{n} \times \mathbf{m}$ in the space of the old angles. Then, the action J_1, conjugate to ψ_1, is automatically a constant of the motion.

For the canonical transform, we choose a generating function of type 3 in the notation of Goldstein,[16] that is, a function that in our case depends on the old actions and the new angles. We make the ansatz

$$F_3(\mathbf{I},\boldsymbol{\psi}) = -\langle \mathbf{I}, \mathbf{M}\boldsymbol{\psi}\rangle = -\sum_{i,j} I_i M_{ij} \psi_j \tag{18}$$

with some 3×3 matrix $\mathbf{M}$, which we define in the following. Then the new and old phase-space coordinates are related via

$$\phi_i = -\partial F_3/\partial I_i = \sum_j M_{ij}\psi_j, \quad J_i = -\partial F_3/\partial \psi_i = \sum_j M_{ji} I_j \tag{19}$$

that is, when the angles transform with a matrix $\mathbf{M}$, the actions transform with the inverse transpose of $\mathbf{M}$. We require that $\psi_1 \mathbf{m} \times \mathbf{n} = (\phi_1,\phi_2,\phi_3)$. This fixes the first row of $\mathbf{M}$ to $\mathbf{m} \times \mathbf{n}$. Then, the first new action, J_1, which by construction is a constant of the motion, is equal to $\langle \mathbf{n} \times \mathbf{m}, (I_1,I_2,I_3)\rangle$ giving in our case

$$J_1 = 2I_1 + I_2 + 4I_3 \tag{20}$$

In principle, we are free in the choice of the remaining components of the matrix $\mathbf{M}$. In practice, however, we would like the new actions to be related to the old actions in a simple way to have a simple interpretation of these actions. In our case, we require that $J_2 = I_1$ and $J_3 = I_3$, that is, we choose the second and the third row of $\mathbf{M}$ equal to (1,0,0) and (0,0,1). The transformations in eq 19 become

$$\begin{pmatrix} J_1 \\ J_2 \\ J_3 \end{pmatrix} = \mathbf{M}^{\mathrm{T}} \begin{pmatrix} I_1 \\ I_2 \\ I_3 \end{pmatrix} = \begin{pmatrix} 2I_1 + I_2 + 4I_3 \\ I_1 \\ I_3 \end{pmatrix} \tag{21}$$

and

$$\begin{pmatrix} \psi_1 \\ \psi_2 \\ \psi_3 \end{pmatrix} = \mathbf{M}^{-1} \begin{pmatrix} \phi_1 \\ \phi_2 \\ \phi_3 \end{pmatrix} = \begin{pmatrix} \phi_2 \\ \phi_1 - 2\phi_2 \\ \phi_3 - 4\phi_2 \end{pmatrix} \tag{22}$$

Note that the matrix $\mathbf{M}$ defined this way is unimodular, that is, it has integer components and unit determinant. This secures that its inverse again has integer components so that the new angles ψ_i again run over intervals of length 2π. In fact, this gives the new variables, J_i, the meaning of action variables according to the strong definition of action variables as, for example, formulated by Arnold.[5]

The conserved action J_1 for which we will write from now on $\mathscr{P}$ is the classical analogue of the so-called superpolyad number

$$P = 2n_1 + n_2 + 4n_3 \tag{23}$$

with n_1, n_2, and n_3 as the number of quanta in the original degrees of freedom, that is, in the symmetric stretch, in the bend, and in the asymmetric stretch. Because n_2 is the sum of the quanta of two degenerate bend degrees of freedom that have to be the same to have a vanishing vibrational angular momentum, it can assume only even integer values. Incorporating the zero-point energies, the classical superpolyad is quantized according to $\mathscr{P} = P + 4$. The conservation of the superpolyad number was the basis for the construction of the effective quantum Hamiltonian, that is, because of the approximate resonances, in eq 1 the Hamiltonian should have off-diagonal elements, which interchange the quanta between the different degrees of freedom only in such a way that the superpolyad number is conserved. For the classical system, the existence of a conserved quantity simplifies the analysis because it reduces the number of the effective degrees of freedom, in our case from 3 to 2. For a general discussion of how to reduce the degrees of freedom of a spectroscopic Hamiltonian, see the work of M. E. Kellman.[17]

The Hamiltonian $\mathscr{K}$ in terms of the new phase space coordinates (ψ_1, ψ_2, ψ_3, J_1, J_2, J_3) reads

$$\begin{aligned}\mathscr{K}_0^{\mathrm{full}} = {} & \omega_1 J_2 + \omega_2(\mathscr{P} - 2J_2 - 4J_3) + \omega_3 J_3 + x_{11}{J_2}^2 + \\ & x_{12}J_2(\mathscr{P} - 2J_2 - 4J_3) + x_{13}J_2J_3 + x_{22}(\mathscr{P} - 2J_2 - 4J_3)^2 + \\ & x_{23}(\mathscr{P} - 2J_2 - 4J_3)J_3 + x_{33}{J_3}^2 + y_{111}{J_2}^3 + y_{112}{J_2}^2(\mathscr{P} - \\ & 2J_2 - 4J_3) + y_{123}J_2(\mathscr{P} - 2J_2 - 4J_3)J_3 + y_{113}{J_2}^2J_3 + \\ & y_{122}J_2(\mathscr{P} - 2J_2 - 4J_3)^2 + y_{133}J_2{J_3}^2 + y_{222}(\mathscr{P} - 2J_2 - \\ & 4J_3)^3 + y_{223}(\tilde{P} - 2J_2 - 4J_3)^2J_3 + y_{233}(\mathscr{P} - 2J_2 - 4J_3){J_3}^2 + \\ & y_{333}{J_3}^3 \end{aligned} \tag{24}$$

plus

$$\begin{aligned}\mathscr{K}_1^{\mathrm{full}} = {} & 2(\mathscr{P} - 2J_2 - 4J_3)(F_{\mathrm{e}}^{(2)}\sqrt{J_2} + F_1^{(2)}{J_2}^{3/2} + 2F_2^{(2)}(\mathscr{P} - \\ & 2J_2 - 4J_3)\sqrt{J_2} + F_3^{(2)}\sqrt{J_2}J_3)\cos\psi_2 + 2(F_{\mathrm{e}}^{(3)}J_2\sqrt{J_3} + \\ & F_1^{(3)}{J_2}^2\sqrt{J_3} + F_2^{(3)}J_2\sqrt{J_3}(\mathscr{P} - 2J_2 - 4J_3) + \\ & F_3^{(3)}{J_{\mathrm{b}}}^{3/2}J_2)\cos(2\psi_2 - \psi_3) + 2(\mathscr{P} - 2J_2 - 4J_3)(F_{\mathrm{e}}^{(4)}\sqrt{J_2J_3} + \\ & F_1^{(4)}{J_2}^{3/2}\sqrt{J_3} + F_2^{(4)}(\mathscr{P} - 2J_2 - 4J_3)\sqrt{J_2J_3} + \\ & F_3^{(4)}{J_3}^{3/2}\sqrt{J_2})\cos(\psi_2 - \psi_3) + 2F^{(10)}\sqrt{J_3}(\mathscr{P} - 2J_2 - \\ & 4J_3)^2\cos\psi_3 + 2F^{(11)}J_2(\mathscr{P} - 2J_2 - 4J_3)^2\cos(2\psi_2) + \\ & 2F^{(12)}{J_2}^2J_3\cos(4\psi_2 - 2\psi_3) + 2F^{(13)}{J_2}^{3/2}\sqrt{J_3}(\mathscr{P} - 2J_2 - \\ & 4J_3)\cos(3\psi_2 - \psi_3) \end{aligned} \tag{25}$$

all of which is parametric in J_1.

The numerical values for the parameters of the effective Hamiltonian are taken from the eighth row of Table 3 in the work of Teffo, Perevalov, and Lyulin,[2] which we list once more in Table 1 of this work. The relatively large size of the parameter $F_{\mathrm{e}}^{(2)} = -17.9632$ indicates on the first inspection that the 1:2 Fermi resonance of the symmetric stretch and the bend should have a dominating effect on the quantum mechanics as well as on the classical mechanics. That this is indeed the case can be proven to be correct by various considerations. In Figure 1 the amplitudes, $\langle s,P|n_1,n_2,n_3\rangle$, of the normal-mode basis states, $|n_1,n_2,n_3\rangle$ (which are the eigenstates of the unperturbed effective Hamiltonian with $\hat{H}_1 = 0$) for the eigenstates, $|P,s\rangle$, of the full effective Hamiltonian are shown for $P = 14$. Here, s counts the eigenstates with a fixed superpolyad number P ordered according to magnitude in energy. Let us remark that the superpolyad number has to be even and that the number of eigenstates in a superpolyad P is

$$N(P) = \begin{cases} P^2/16 + P/2 + 1 & \text{if } P/2 \text{ is even} \\ P^2/16 + \mathrm{P}/2 + {}^3/_4 & \text{if } P/2 \text{ is odd} \end{cases} \tag{26}$$

giving $N(14) = 20$ and $N(22) = 42$. The figure shows two important things. First, it proves that it is generally not reasonable to assign normal-mode quantum numbers (n_1, n_2, n_3) to the states $|P,s\rangle$. As a reasonable limit for the ability to assign normal-mode quantum numbers to an eigenstate, the criterion can be taken that $|P,s\rangle$ should have at least a 50%

TABLE 1: Parameters of the Spectroscopic Hamiltonian

ω_1	ω_2	ω_3	x_{11}	x_{12}	x_{13}	x_{22}
1298.590 11	596.2937	2281.998 14	−3.9178	−3.0087	−27.207 21	0.5432
x_{23}	x_{33}	y_{111}	y_{112}	y_{113}	y_{122}	y_{123}
−14.585 13	−15.165 16	−0.004 714	−0.116 084	−0.343 11	−0.035 329	0.515 13
y_{133}	y_{222}	y_{223}	y_{233}	y_{333}	$F_e^{(2)}$	$F_1^{(2)}$
0.059 79	−0.013 188 7	0.046 411	0.009 261	0.015 737	−17.963 240	0.2365
$F_2^{(2)}$	$F_3^{(2)}$	$F_e^{(3)}$	$F_1^{(3)}$	$F_2^{(3)}$	$F_3^{(3)}$	$F_e^{(4)}$
0.3899	0	−0.329 69	−0.265 334	1.009 89	1.9716	0
$F_1^{(4)}$	$F_2^{(4)}$	$F_3^{(4)}$	$F^{(10)}$	$F^{(11)}$	$F^{(12)}$	$F^{(13)}$
0	0	−0.229 66	0	0	0	0.233 32

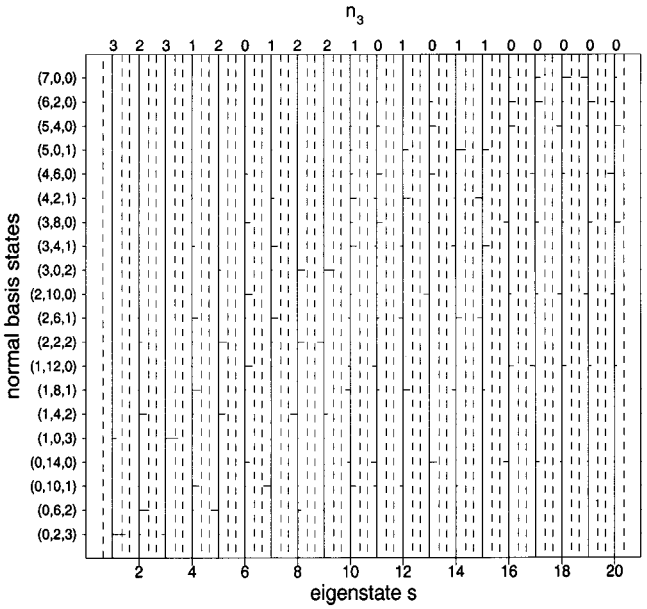

Figure 1. Amplitudes $\langle P,s|n_1,n_2,n_3\rangle$ (horizontal ticks) of the basis states for the eigenstates of superpolyad $P = 14$. The dashed lines bounding each solid line mark a "confidence interval" of width $2/\sqrt{2}$. On the abscissa, s labels the states within the superpolyad ordered according to magnitude in energy. The numbers above are the quantum numbers n_3, which can be approximately assigned to the quantum states $|P,s\rangle$.

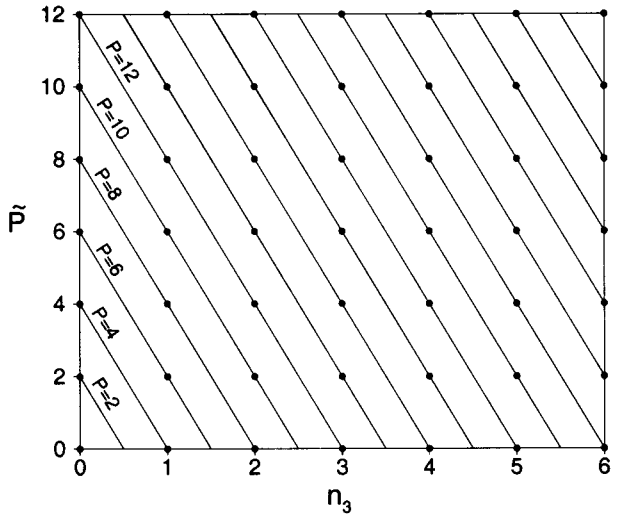

Figure 2. Distribution of the eigenstates (dots) of the one-resonance system with polyad number $\tilde{P}$ and quantum number n_3 over the states of the full system, which incorporates all resonances with superpolyad number P. Note that each dot in each line of constant $\tilde{P}$ represents $\tilde{P}/2 + 1$ eigenstates.

contribution from the corresponding basis state $|n_1,n_2,n_3\rangle$.[18] This is only the case for very few eigenstates of superpolyad 14 and for almost no eigenstates of superpolyad 22 for which we omit the presentation of a separate figure. Second, Figure 1 shows that only those normal basis states that have the same quantum number n_3 mix for a given eigenstate $|P,s\rangle$. To a great extent, this even holds for superpolyad $P = 22$. Accordingly, to a very high degree of approximation, n_3 is a further good quantum number besides the superpolyad number, that is, the superpolyad blocks of the matrix representation of the quantum Hamiltonian in terms of the basis set $\{|n_1,n_2,n_3\rangle\}$ can be further block diagonalized so that each block corresponds to a fixed quantum number n_3. For a system in which one quantum number can be separated off, it is common to deal with a polyad number that is a linear combination of the those quantum numbers that are no longer good quantum numbers. We define the polyad number

$$\tilde{P} = P - 4n_3 = 2n_1 + n_2 \tag{27}$$

so that we are left with two good quantum numbers n_3 and $\tilde{P}$. Like the superpolyad number P, the polyad number $\tilde{P}$ can only assume even integer values. The number of states in a polyad $\tilde{P}$ does not depend on n_3 and is given by

$$\tilde{N}(\tilde{P}) = \tilde{P}/2 + 1 \tag{28}$$

Figure 2 shows how the superpolyads P are distributed over the polyads $\tilde{P}$ and the blocks with fixed n_3.

The approximate separability of n_3, of course, also further simplifies the analysis of the classical system. If we neglect all of the resonances up to the 1:2 resonance between the symmetric stretch and the bend, then the action I_3 and the classical analogue of the polyad $\tilde{P}$,

$$\tilde{\mathscr{P}} = 2I_1 + I_2 \tag{29}$$

are two constants of the classical motion besides the total energy so that the classical system is integrable. To describe the integrable system, we change to the new actions

$$\begin{pmatrix}\tilde{J}_1\\ \tilde{J}_2\\ \tilde{J}_3\end{pmatrix} = \begin{pmatrix}2I_1 + I_2\\ I_1\\ I_3\end{pmatrix} = \tilde{\mathbf{M}}^{\mathrm{T}}\begin{pmatrix}I_1\\ I_2\\ I_3\end{pmatrix} \tag{30}$$

that is, $\tilde{J}_1$ is the polyad $\tilde{\mathscr{P}}$ and $\tilde{J}_3$ remains the conserved third action, I_3. The angles transform with the inverse of the matrix, $\tilde{\mathbf{M}}$, giving

$$\begin{pmatrix}\tilde{\psi}_1\\ \tilde{\psi}_2\\ \tilde{\psi}_3\end{pmatrix}=\tilde{\mathbf{M}}^{-1}\begin{pmatrix}\phi_1\\ \phi_2\\ \phi_3\end{pmatrix}=\begin{pmatrix}\phi_2\\ \phi_1-2\phi_2\\ \phi_3\end{pmatrix} \tag{31}$$

The classical Hamiltonian in terms of the phase-space variables $(\tilde{\boldsymbol{\psi}},\tilde{\mathbf{J}})$ is given by

$$\begin{aligned}\mathscr{K}_0^{\text{one}} = {}& \omega_1\tilde{J}_2+\omega_2(\tilde{\mathscr{P}}-2\tilde{J}_2)+\omega_3\tilde{J}_3+x_{11}\tilde{J}_2{}^2+x_{12}\tilde{J}_2(\tilde{\mathscr{P}}-\\ & 2\tilde{J}_2)+x_{13}\tilde{J}_2\tilde{J}_3+x_{22}(\tilde{\mathscr{P}}-2\tilde{J}_2)^2+x_{23}(\tilde{\mathscr{P}}-2\tilde{J}_2)\tilde{J}_3+\\ & x_{33}\tilde{J}_3{}^2+y_{111}\tilde{J}_2{}^3+y_{112}\tilde{J}_2{}^2(\tilde{\mathscr{P}}-2\tilde{J}_2)+y_{123}\tilde{J}_2(\tilde{\mathscr{P}}-2\tilde{J}_2)\tilde{J}_3+\\ & y_{113}\tilde{J}_2{}^2\tilde{J}_3+y_{122}\tilde{J}_2(\tilde{\mathscr{P}}-2\tilde{J}_2)^2+y_{133}\tilde{J}_2\tilde{J}_3{}^2+y_{222}(\tilde{\mathscr{P}}-\\ & 2\tilde{J}_2)^3+y_{223}(\tilde{\mathscr{P}}-2\tilde{J}_2)^2J_3+y_{233}(\tilde{\mathscr{P}}-2J_2)\tilde{J}_3{}^2+y_{333}\tilde{J}_3{}^3\end{aligned} \tag{32}$$

plus the interaction term

$$\begin{aligned}\mathscr{K}_1^{\text{one}} = {}& 2(\tilde{\mathscr{P}}-2\tilde{J}_2)(F_{\text{e}}^{(2)}\sqrt{\tilde{J}_2}+F_1^{(2)}\tilde{J}_2{}^{3/2}+F_2^{(2)}(\tilde{\mathscr{P}}-\\ & 2\tilde{J}_2)\sqrt{\tilde{J}_2}+F_3^{(2)}\sqrt{\tilde{J}_2}\tilde{J}_3)\cos\tilde{\psi}_2\end{aligned} \tag{33}$$

The system described by $\mathscr{K}^{\text{one}}$ is effectively a one degree of freedom system in the canonical variables (J_2, ψ_2). In Table 2, we list the energy spectrum obtained from the quantum Hamiltonian with all of the resonances together with the assignment in terms of the quantum numbers of the one-resonance system, which is the subject of the following two sections.

3. N_2O with Only the 1_s:2_b Fermi Resonance

As mentioned above, in the one-resonance approximation, the classical dynamics is integrable. We can discuss the integrable system from different perspectives: First, it is a three degree of freedom system with phase-space coordinates $(\tilde{\psi}_1, \tilde{\psi}_2, \tilde{\psi}_3, \tilde{J}_1, \tilde{J}_2, \tilde{J}_3)$ where $\tilde{\psi}_1$ and $\tilde{\psi}_3$ are cyclic variables, that is, they do not appear in the Hamiltonian $\mathscr{K}^{\text{one}}$and therefore the conjugate momentum variables $\tilde{J}_1$ and $\tilde{J}_3$ are constants of the motion. Second, we can treat the system as a family of two degree of freedom systems parametrized by the conserved action $\tilde{J}_3$ with phase-space variables $(\tilde{\psi}_1, \tilde{\psi}_2, \tilde{J}_1, \tilde{J}_2)$. Third, we can consider the system as a two-parameter family of one degree of freedom systems with family parameters, $\tilde{J}_1$and $\tilde{J}_3$, and phase-space variables $(\tilde{\psi}_2, \tilde{J}_2)$. In the following, we will mainly adopt the latter point of view and we will, for short, write $(\tilde{\psi}, \tilde{J})$ instead of $(\tilde{\psi}_2, \tilde{J}_2)$.

The phase space of an integrable system with three degrees of freedom is foliated by invariant 3-tori. The energy eigenstates tend to concentrate on those 3-tori the actions of which fulfill the EBK quantization conditions. In our case, $\tilde{J}_1$ and $\tilde{J}_3$ are quantized with $\tilde{P}+2$ and $n_3+{}^1/_2$, respectively, giving two of the three EBK quantization conditions that define the quantized 3-torus. The third EBK quantization condition is

$$\frac{1}{2\pi}\oint\tilde{J}_2\,\mathrm{d}\tilde{\psi}_2\equiv\frac{1}{2\pi}\int_0^{2\pi}\tilde{J}_2\,\mathrm{d}\tilde{\psi}_2=\tilde{n}_2+\frac{1}{2} \tag{34}$$

Interpreting our system as a one degree of freedom system, we can plug the quantized values for the parameters $\tilde{J}_1$ and $\tilde{J}_3$ into the classical Hamiltonian $\mathscr{K}^{\text{one}}$ and display the "quantizing trajectories" in the phase portrait $(\tilde{\psi}_2, \tilde{J}_2) \equiv (\tilde{\psi}, \tilde{J})$. The quantizing trajectories are defined as the level sets of $\mathscr{K}^{\text{one}}$ set equal to the quantum mechanical energy eigenvalues. Figure 3 shows the quantizing trajectories of polyads $\tilde{P}=14$ with $n_3=0$ and the corresponding $\tilde{N}(14)=8$ energy eigenvalues of Table 2.

The quantizing trajectories fall into three groups. If we consider the term $\mathscr{K}_1^{\text{one}}$ as an integrable perturbation of $\mathscr{K}_0^{\text{one}}$ and refer to the tori of the system described by $\mathscr{K}_0^{\text{one}}$ alone as the primary tori, one can say that states 3−6 of polyad $\tilde{P}=14$ correspond to deformed primary tori. Note that the tori of $\mathscr{K}_0^{\text{one}}$ alone would appear as horizontal lines in the phase portrait $(\tilde{\psi}, \tilde{J})$. Because of the integrable perturbation $\mathscr{K}_1^{\text{one}}$, there appear two new regions of which the centers are elliptic points of the one degree of freedom system, which are denoted by e_1 and e_2 in Figure 3. The tori about e_1, which correspond to the states $s=1$ and $s=2$, and e_2, which correspond to states 7 and 8, will be referred to as secondary tori. At first, it seems as if there were two separatrices: a first separatrix separating the secondary tori about e_1 and the primary tori and a second separatrix separating the primary tori and the secondary tori about e_2. They are indicated by dashed lines in Figure 3. In the following, we will see that the first separatrix is not a separatrix in the sense that it is connected to unstable motion. In fact, the secondary tori about e_1 transform smoothly to the primary tori. To see this, let us interpret the integrable system as a two degree of freedom system with a parameter J_3, that is, let us forget about the asymmetric stretch for a moment. At the top of the $(\tilde{\psi}, \tilde{J})$ phase portrait, $\tilde{J}_1$ reaches its maximum value, $\tilde{\mathscr{P}}/2$. This implies that the original action I_2 vanishes while I_1 reaches its maximum, $\tilde{\mathscr{P}}/2$. Accordingly, the whole top line of the phase portrait represents a single symmetric stretch periodic orbit of the two degree of freedom system. Conversely, at the bottom of the $(\tilde{\psi}, \tilde{J})$ phase portrait, $\tilde{J}$ vanishes and, accordingly, the original action I_1 vanishes while the original action I_2 reaches its maximum value, which is equal to $\tilde{\mathscr{P}}$. The whole bottom line represents a single bend periodic orbit of the two degree of freedom system. In contrast to that, the circles of the $(\tilde{\psi}, \tilde{J})$ phase portrait correspond to 2-tori in phase space of the two degree of freedom system. From the perspective of the one degree of freedom system, the top and the bottom line each represent a single point. Taking into account the periodic boundary condition in the ψ direction, the phase portrait $(\tilde{\psi}, \tilde{J})$ has the topology of a sphere. If we want to present the dynamics on a "true" sphere by some change of coordinates, it is to be taken into account that the change of coordinates must be canonical to preserve the form of Hamilton's equations of the motion and to preserve the ability to draw any conclusion on the original system. For a one degree of freedom system, this means that the transformation has to be area preserving. This leads one to the map

$$\varphi=\tilde{\psi},\quad \vartheta=\arccos\left(\frac{\tilde{\mathscr{P}}-4\tilde{J}}{\tilde{\mathscr{P}}}\right) \tag{35}$$

where $\varphi\in[0,2\pi]$ and $\vartheta\in[0,\pi]$ are the usual angles on a sphere $(x,y,z)=(R\cos\varphi\sin\theta, R\sin\varphi\sin\theta, R\cos\theta)$, which is the so-called "polyad sphere" invented by M. E. Kellman and co-workers.[19−22] If the radius of the sphere is chosen to be equal to $R=\sqrt{\tilde{\mathscr{P}}}2$ one immediately proves the area preserving property, $\mathrm{d}\tilde{\psi}\,\mathrm{d}\tilde{J}=R^2\sin\vartheta\,\mathrm{d}\vartheta\,\mathrm{d}\varphi$. Following eq 34, the top of the (ψ, J) phase portrait maps to the south pole and the bottom maps to the north pole.

In Figure 4, the polyad sphere is shown for polyad $\tilde{P}=14$ and $n_3=0$ with the quantizing trajectories of Figure 3. On the polyad sphere, the "separatrix" between states 2 and 3 maps to a smooth circle, which runs smoothly across the north pole. The reason for the smoothness is that in the $(\tilde{\psi}, \tilde{J})$ phase portrait the "separatrix" intersects the bottom line $\tilde{J}=0$ perpendicularly at $\tilde{\psi}=\pi\pm\pi/2$. Accordingly, the secondary tori about e_1 transform smoothly to the primary tori. The separatrix between

TABLE 2: Energy Levels, E^{full}, of the Spectroscopic Hamiltonian Which Includes All of the Resonances for Superpolyads $P = 14$ and $P = 22$ and the Assignment in Terms of the Quantum Numbers of the One-Resonance Hamiltonian[a]

E^{full} (cm^{-1})	(P, s)	$E^{one\ b}$ (cm^{-1})	$(\tilde{P}, n_3, \tilde{s})$	torus[c]	E^{full} (cm^{-1})	(P, s)	$E^{one\ b}$ (cm^{-1})	$(\tilde{P}, n_3, \tilde{s})$	torus[c]
10 032.0	(14, 1)	10 033.2	(2, 3, 1)	p	14 600.2	(22, 12)	14 601.0	(10, 3, 3)	p
10 089.3	(14, 2)	10 091.3	(6, 2, 1)	e_1	14 721.2	(22, 13)	14 711.8	(22, 0, 1)	e_1
10 149.5	(14, 3)	10 149.9	(2, 3, 2)	p	14 724.6	(22, 14)	14 725.2	(10, 3, 4)	p
10 189.6	(14, 4)	10 190.7	(10, 1, 1)	e_1	14 729.5	(22, 15)	14 727.0	(18, 1, 2)	e_1
10 240.8	(14, 5)	10 241.6	(6, 2, 2)	p	14 736.4	(22, 16)	14 735.5	(14, 2, 3)	p
10 330.3	(14, 6)	10 327.1	(14, 0, 1)	e_1	14 818.9	(22, 17)	14 819.4	(10, 3, 5)	p
10 360.4	(14, 7)	10 360.9	(10, 1, 2)	p	14 881.4	(22, 18)	14 882.6	(14, 2, 4)	p
10 365.2	(14, 8)	10 365.6	(6, 2, 3)	p	14 894.5	(22, 19)	14 896.8	(10, 3, 6)	e_2
10 450.8	(14, 9)	10 451.3	(6, 2, 4)	p	14 901.6	(22, 20)	14 902.8	(18, 1, 3)	e_1
10 512.5	(14, 10)	10 513.5	(10, 1, 3)	p	14 918.9	(22, 21)	14 909.8	(22, 0, 2)	e_1
10 515.5	(14, 11)	10 513.3	(14, 0, 2)	e_1	15 009.2	(22, 22)	15 010.7	(14, 2, 5)	p
10 643.4	(14, 12)	10 644.0	(10, 1, 4)	p	15 065.9	(22, 23)	15 066.9	(18, 1, 4)	p
10 686.6	(14, 13)	10 685.9	(14, 0, 3)	p	15 103.0	(22, 24)	15 098.9	(22, 0, 3)	e_1
10 743.3	(14, 14)	10 744.1	(10, 1, 5)	p	15 110.8	(22, 25)	15 112.9	(14, 2, 6)	p
10 820.1	(14, 15)	10 821.5	(10, 1, 6)	e_2	15 192.2	(22, 26)	15 196.0	(14, 2, 7)	e_2
10 842.9	(14, 16)	10 842.6	(14, 0, 4)	p	15 215.8	(22, 27)	15 217.0	(18, 1, 5)	p
10 980.4	(14, 17)	10 980.1	(14, 0, 5)	p	15 279.6	(22, 28)	15 278.0	(22, 0, 4)	e_1
11 092.6	(14, 18)	11 092.0	(14, 0, 6)	p	15 290.5	(22, 29)	15 297.4	(14, 2, 8)	e_2
11 178.2	(14, 19)	11 177.1	(14, 0, 7)	e_2	15 348.5	(22, 30)	15 350.3	(18, 1, 6)	p
11 274.9	(14, 20)	11 272.4	(14, 0, 8)	e_2	15 446.5	(22, 31)	15 446.0	(22, 0, 5)	p
14 210.4	(22, 1)	14 215.7	(2, 5, 1)	p	15 458.7	(22, 32)	15 460.8	(18, 1, 7)	p
14 226.7	(22, 2)	14 229.5	(6, 4, 1)	e_1	15 546.1	(22, 33)	15 548.9	(18, 1, 8)	e_2
14 287.0	(22, 3)	14 292.2	(10, 3, 1)	e_1	15 601.8	(22, 34)	15 601.2	(22, 0, 6)	p
14 330.6	(22, 4)	14 332.9	(2, 5, 2)	p	15 644.7	(22, 35)	15 648.5	(18, 1, 9)	e_2
14 374.3	(22, 5)	14 376.4	(6, 4, 2)	p	15 742.6	(22, 36)	15 741.2	(22, 0, 7)	p
14 393.6	(22, 6)	14 398.5	(14, 2, 1)	e_1	15 765.9	(22, 37)	15 771.2	(18, 1, 10)	e_2
14 452.8	(22, 7)	14 455.1	(10, 3, 2)	p	15 864.2	(22, 38)	15 861.7	(22, 0, 8)	p
14 496.6	(22, 8)	14 497.3	(6, 4, 3)	p	15 961.3	(22, 39)	15 957.4	(22, 0, 9)	p
14 540.5	(22, 9)	14 541.0	(18, 1, 1)	e_1	16 057.8	(22, 40)	16 051.1	(22, 0, 10)	e_2
14 571.5	(22, 10)	14 573.3	(14, 2, 2)	e_1	16 178.1	(22, 41)	16 167.9	(22, 0, 11)	e_2
14 580.5	(22, 11)	14 580.7	(6, 4, 4)	p	16 317.0	(22, 42)	16 303.5	(22, 0, 12)	e_2

[a] The energies are internal energies, that is, they include the ground-state energy. [b] The corresponding levels calculated from the one-resonance Hamiltonian. [c] The type of torus on which the wave functions condense (see section 4).

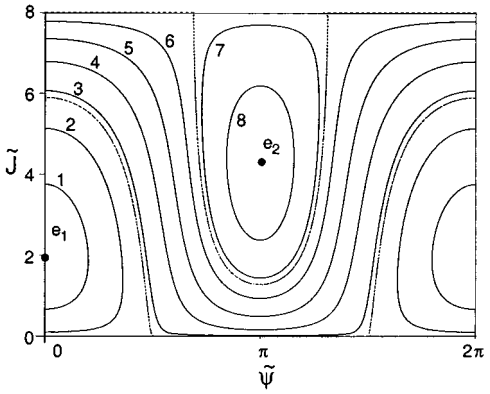

Figure 3. Phase portraits ($\tilde{\psi}$, $\tilde{J}$) for $\tilde{\mathscr{H}} = 16$ ($\tilde{P} = 14$) and $I_3 = {}^1/_2$ ($n_3 = 0$).

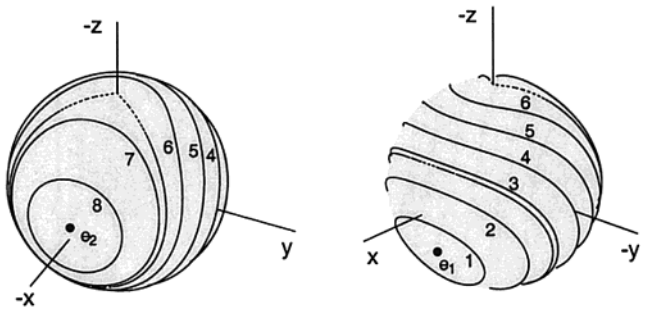

Figure 4. Polyad sphere for $\tilde{P} = 14$ and $n_3 = 0$ with the quantizing trajectories of Figure 3.

the primary tori and the secondary tori about e_2 maps to a circle with a cusp at the south pole.

The polyad sphere is not only introduced for esthetic reasons, but the fact that phase space of the one degree freedom system ($\tilde{\psi}$, $\tilde{J}$) has the topology of a sphere has important implications. The most striking one is the limitation on the number of periodic orbits of different stability due to the Poincaré index theorem. If each (isolated) periodic orbit, po, is mapped to a stability index, σ, according to

$$\sigma_{po} = \begin{cases} 1 & \text{if po is stable} \\ -1 & \text{if po is unstable} \\ 0 & \text{if po is unstable cusp orbit} \end{cases} \tag{36}$$

then the Poincaré index theorem tells that

$$\sum_{po} \sigma_{po} = 2 \tag{37}$$

The role of the unstable cusp orbit is special because it corresponds to a singularity of the polar coordinates in which the isotropic oscillator of the degenerate bend degrees of freedom is separated. We will shortly come back to this point. Equation 37 is consistent with our result of two elliptic points, e_1 and e_2, and one cusp.

In Figure 5, we show how far the quantizing trajectories fulfill the EBK quantization condition in eq 33. The figure shows the effective quantum number

$$\tilde{n}_2^{eff} \equiv \frac{1}{2\pi} \oint \tilde{J}\, d\tilde{\psi} - \frac{1}{2} \tag{38}$$

where the integrals are taken along the quantizing trajectories. The EBK quantization condition in eq 33 is discontinuous at the separatrix because of the discontinuity of the action defined

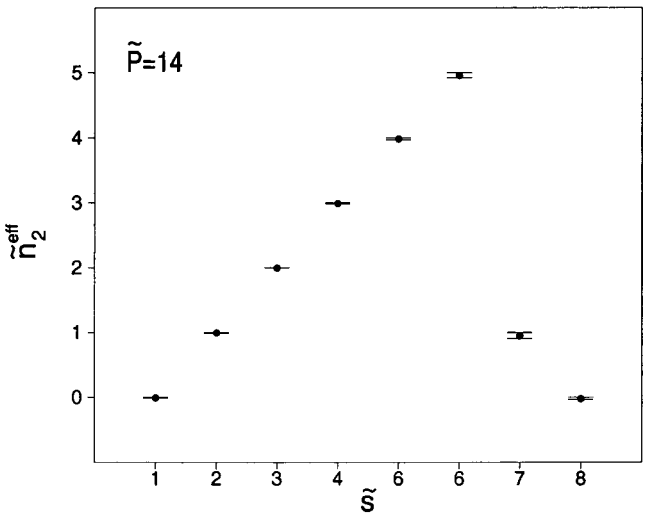

Figure 5. Effective quantum numbers of eq 37 for the quantizing trajectories of Figure 3. The bars indicate the differences to integer values.

in eq 33. This causes the jumps of $\tilde{n}_{\mathrm{eff}}$ in Figure 5 between states 6 and 7 for polyad 14. The agreement with integer values is very good. It becomes only a little bit worse for states close to the separatrix, which is a feature generally faced in the EBK quantization of integrable systems with separatrices. In such a case, the semiclassical quantization has to be improved by a so-called uniformization,[23,24] which we will not perform here.

To see the meaning of the quantum number $\tilde{n}_2$, let us have a look at the wave functions in the space of the normal coordinates, q_i. They are given by

$$\Psi^{\mathrm{norm}}_{(\tilde{P},n_3,\tilde{s})}(q_1,q_2,q_3) = \sum_{n_1,n_2}{}' \tilde{a}_{(\tilde{P},n_3,\tilde{s}),(n_1,n_2,n_3)} \Psi_{n_1}(q_1)\Psi^{(\mathrm{r})}_{n_2/2}(q_2)\Psi_{n_3}(q_3) \quad (39)$$

where Ψ_n is the nth wave function of a one-dimensional harmonic oscillator, $\Psi^{(\mathrm{r})}_n$ is the nth radial wave function of a two-dimensional isotropic harmonic oscillator (see the work of Joyeux[25] for the details), and the amplitudes are the matrix elements $\tilde{a}_{(\tilde{P},n_3,\tilde{s}),(n_1,n_2,n_3)} \equiv \langle \tilde{P},n_3,\tilde{s}|n_1,n_2,n_3\rangle$. The prime at the summation symbol means that the summation runs over all n_1 and n_2 with $2n_1 + n_2 = \tilde{P}$.

In Figure 6, we represent the projections of the wave functions of eq 38 for the eigenstates of polyad $\tilde{P} = 14$ with $n_3 = 0$. For comparison, we also show the projections of classical trajectories started on the corresponding quantized tori where the solutions of Hamilton's equations of the motions in action angle variables are lifted back to the original normal coordinates via

$$q_i(t) = \sqrt{2I_i(t)}\cos(\phi_i(t)) \quad (40)$$

As mentioned in the Introduction, the trajectories obtained by eq 39 are, in practice, generally very close to the true trajectories in the original coordinates. As expected, the quantum classical correspondence is very transparent. State $\tilde{s} = 1$ is localized on a thin torus, which surrounds the periodic orbits corresponding to the elliptic point e_1. At e_1, the angle $\tilde{\psi}_2$ is locked at 0. With the use of eq 31, this gives $\phi_2 = \phi_1/2$, which leads to a left open "u" shaped periodic orbit in the space of the normal coordinates (q_1, q_2). The quantum number $\tilde{n}_2$ can be considered as the excitation perpendicular to this periodic orbit. The excitation along the periodic orbit is related to $\tilde{P} - \tilde{n}_2$. In accordance with our statement above, the projections of the tori change smoothly across the pseudoseparatrix between eigenstates $\tilde{s} = 2$ and $\tilde{s} = 3$. In contrast to that, the projections of the tori change discontinuously across the true separatrix between eigenstates $\tilde{s} = 6$ and $\tilde{s} = 7$. Between the two states, one classically finds an unstable periodic orbit running along the q_1 axis. This is the periodic orbit that corresponds to the cusp on the polyad sphere in Figure 4. The state $\tilde{s} = 8$ corresponding to the largest energy in polyad $\tilde{P} = 14$ with $n_3 = 0$ is localized on a thin torus surrounding the periodic orbit that corresponds to the elliptic point e_2. Here, $\tilde{\psi}_2$ is locked at π or $\phi_2 = \phi_1/2 + \pi/2$, which gives a right open "u" shaped periodic orbit.

The complete wave function in the three-dimensional space of the normal coordinates q_i is obtained from the multiplication of the wave functions represented in Figure 6 by a harmonic oscillator wave function with quantum number n_3 and argument q_3. Accordingly, n_3 counts the number of nodal surfaces parallel to the planes (q_1, q_2) in Figure 6.

The bifurcation diagram, which is shown in Figure 7, divides the plane $(\tilde{J}_3, \tilde{\mathscr{P}})$ into two regions, which we denote by I and II, where we follow the general classification scheme of bifurcation diagrams for 1:2 Fermi resonance systems given by Svitak, Rose, and Kellman.[26] In region I, there is no true separatrix and there are two elliptic points on the polyad sphere, of which both are located on the longitude, $\varphi = 0$. One of them corresponds to the elliptic point e_1 shown in Figure 4 and is located away from the poles. The other one corresponds to the top line of phase portrait $(\tilde{\psi}, \tilde{J})$ in this parameter range and is located at the south pole. In region II, one faces the situation already shown in Figure 4, that is, there are two elliptic points both located away from the poles on the longitude $\varphi = 0$ and a separatrix connected to a cusp at the south pole. Because quantum mechanically $\tilde{\mathscr{P}}$ can only assume even integer values and the line separating regions I and II is rather flat, one can say that in the energy range where the one-resonance approximation is valid the polyad spheres for polyad numbers $\tilde{P} = 0$ or $\tilde{P} = 2$, independently of n_3, have no separatrix. According to Figure 7, the situation changes for n_3 of the order of 30, which lie beyond the applicability of one resonance approximation.

For quantum mechanics, the size of structures in phase space compared to Planck's constant is essential. The bifurcation diagram in Figure 7 does not give information on how in region II the quantizing trajectories of the quantum states are distributed relative to the separatrix. We therefore show in Figure 8 the location of the eigenstates in diagrams in which energy is plotted against the classical polyad $\tilde{\mathscr{P}}$ for fixed quantum number n_3. Figure 8 shows both the energy of the cusp and the energy of the pseudoseparatrix running through the north pole. Although there already is a separatrix for $\tilde{P} = 4$, the first eigenstate located on a secondary torus about e_2 appears for polyad $\tilde{P} = 8$. This holds at least for $0 \le n_3 \le 3$. Similarly, the first eigenstates located on secondary tori about e_1 appear for $\tilde{P} = 6$ for all $0 \le n_3 \le 3$. The number of eigenstates associated with primary tori decreases with increasing quantum numbers, $\tilde{P}$ and n_3.

4. The Full System

Let us now incorporate all of the resonances and turn to the Hamiltonian $\mathscr{H}^{\mathrm{full}}$ of eqs 24 and 25. We want to read this Hamiltonian as the integrable Hamiltonian $\mathscr{H}^{\mathrm{one}}$, which includes only the dominant resonance term discussed in the preceding section plus a perturbation, which incorporates all of the other resonance terms. This perturbation destroys the integrability.

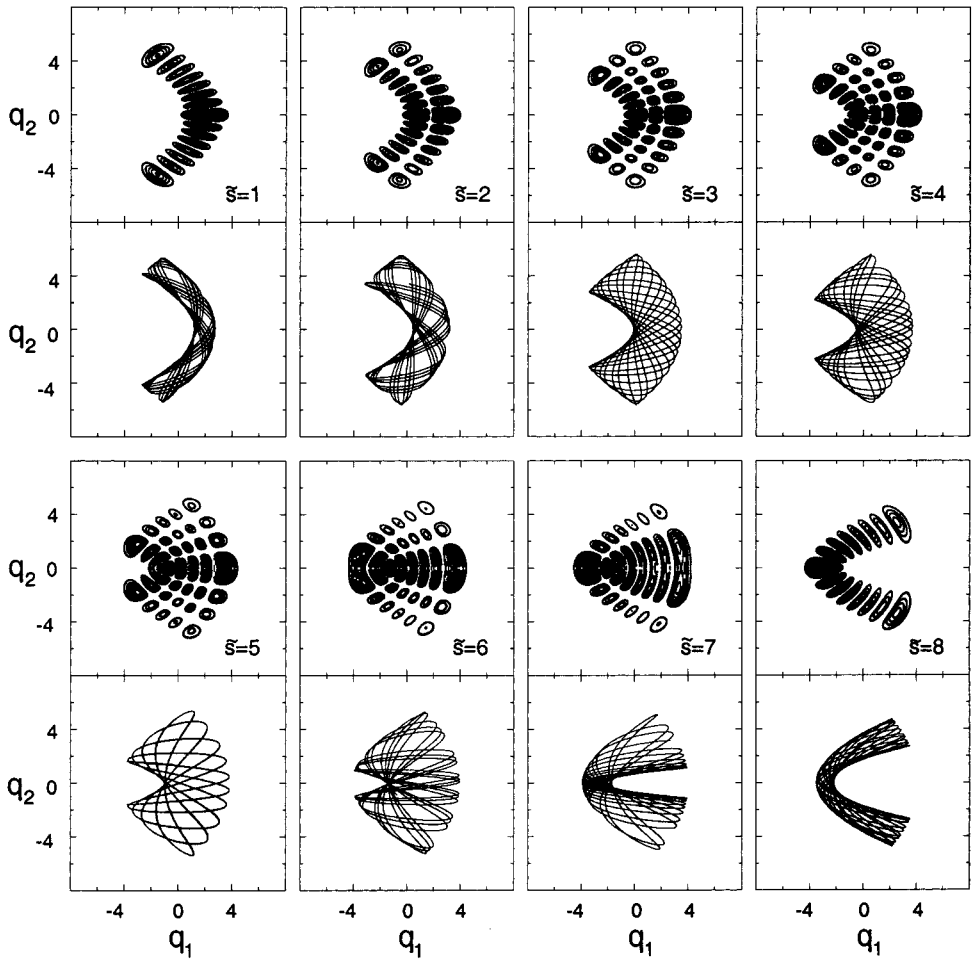

Figure 6. Projection of probability densities of the wave functions $\Psi^{\text{norm}}_{(\tilde{P},n_3,\tilde{s})}$ of eq 38 and of trajectories of the corresponding classical tori to the plane of the normal coordinates q_1 and q_2 for polyad $\tilde{P} = 14$ with $n_3 = 0$. Each trajectory is integrated for a period of time equal to 0.1.

As expected for low and intermediate superpolyad numbers, classical phase space is still very regular as can be seen from Poincaré surfaces of section. Instead of showing Poincaré surfaces of section of superpolyad $P = 14$ for different energies, we show in Figure 9 a superposition of those sets of points that are obtained from starting on the quantized tori of Figure 3, that is, with initial condition $J_3 = {}^1/_2$. This figure is meaningful because the tori are only slightly distorted by the other resonances so that there are no intersections. The similarity of Figures 9 and 3 demonstrates that the quantum states of the full system with moderate superpolyad numbers can still be assigned in terms of the EBK quantum numbers of the quantized tori of section 3.

Classically, the situation is different for $P = 22$ where noticeable features of chaos arise in phase space and a figure analogous to Figure 9 is no longer meaningful. Instead, we show in Figure 10 usual Poincaré surfaces of section for different energies. We see that the energetic bottom and top of the superpolyad still correspond to the elliptic points e_1 and e_2 discussed in section 3. Chaos spreads out from the separatrix between these two regular phase-space regions. The chaos band is mainly concentrated about the direct neighborhood of the former separatrix, and it becomes largest in the middle of the superpolyad. But even for intermediate energies, there are always large regular regions away from the chaos band. These regions are so large that there is reason to believe that they will host most of the quantum states and that only a small number of the quantum states will be noticeably influenced by the chaos band. To check this, we again have to look at the quantum mechanical wave functions. The question arises as to which variables to use to represent the wave functions. Because for the full system the asymmetric stretch cannot be separated off, we would have to look at three-dimensional wave functions if we, for example, would represent them with respect to the normal coordinates q_i. This is very inconvenient because on one hand the corresponding plots are difficult to produce and on the other hand the need of two-dimensional pictures requires some kind of projection or cut by which essential information often gets lost. In practice, it is very hard or even impossible to classify the states from such plots. Instead, we find it useful to stay with the configuration space parametrized by the angle variables of our classical analysis. Although this space has the disadvantage of being rather abstract, it has one great advantage that makes it superior to any other configuration space: in angle variables only, the trivial degree of freedom corresponding to the superpolyad number can be separated off, that is, only for the angle coordinates, it is possible to reduce the dimensions. This advantage cannot be overemphasized. Quantum mechanical wave functions in angle space are easily obtained. The representation of the normal basis states $|n_1,n_2,n_3\rangle$ in angle coordinates is given by $\langle\phi_1,\phi_2,\phi_3|n_1,n_2,n_3\rangle = \exp(i(n_1\phi_1 + n_2\phi_2 + n_3\phi_3))/(2\pi)^{3/2}$, which are eigenfunctions of the action operators if we interpret them to be given by $-i\partial/\partial\phi_i$. This is meaningful only in a semiclassical sense but totally sufficient for our considerations. With the matrix elements $a_{(P,s),(n_1,n_2,n_3)} \equiv \langle P,s|n_1,n_2,n_3\rangle$ already shown in Figure 1 for $P = 14$, the

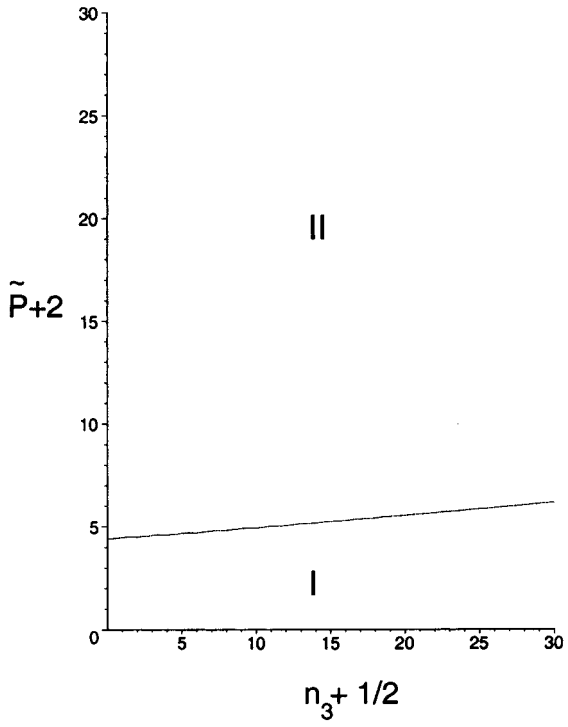

Figure 7. Bifurcation diagram of the one-resonance system. The abscissa is the classical action $\tilde{J}_3 = n_3 + {}^1/_2$. The ordinate is the classical polyad $\tilde{\mathscr{P}} = \tilde{P} + 2$.

representation of the eigenstates $|P,s\rangle$ becomes

$$\Psi^{\mathrm{tor}}_{(P,s)}(\psi_1,\psi_2,\psi_3) \equiv \langle\psi_1,\psi_2,\psi_3|P,s\rangle \tag{41}$$

$$= \sum_{n_1,n_2,n_3}{}' a_{(P,s),(n_1,n_2,n_3)} \langle\psi_1,\psi_2,\psi_3|n_1,n_2,n_3\rangle \tag{42}$$

$$= \mathrm{e}^{iP\psi_1} \frac{1}{(2\pi)^{3/2}} \sum_{n_1,n_2,n_3}{}' a_{(P,s),(n_1,n_2,n_3)}\, \mathrm{e}^{i(n_1\psi_2+n_3\psi_3)} \tag{43}$$

where the factor $\exp(iP\psi_1)$ is just a negligible phase factor wherefore the wave function is effectively a wave function on the two-dimensional toroidal configuration space of the angles ψ_2 and ψ_3. In contrast to eq 38, the summation now also runs over the quantum number n_3. The prime at the summation symbol means that the summation is restricted to those n_i with $2n_1 + n_2 + 4n_3 = P$.

In Figures 11 and 12, the probability densities $|\Psi^{\mathrm{tor}}_{(P,s)}(\psi_2,\psi_3)|^2$ are shown together with the phase $\arg(\Psi^{\mathrm{tor}}_{(P,s)}(\psi_2,\psi_3))$ for a collection of eigenstates of superpolyad $P = 22$. The shaded regions mark phases between 0 and π (mod 2π). The density plots envision that the wave functions are mainly concentrated on strips in direction ψ_3. This is the quantum mechanical manifestation of the classical fact that the action $J_3 = I_3$ approximately remains a constant of the motion and, accordingly, the angle ψ_3 (the asymmetric stretch mode) is approximately decoupled. The mean phase advance in direction ψ_3 divided by 2π, that is, the number of shaded strips (or, equivalently, the number of light strips) that are crossed upon varying ψ_3 from 0 to 2π for constant ψ_2 is the quantum number n_3. Accordingly, we can assign each state $|P,s\rangle$, besides the superpolyad number P, a quantum number n_3. Equivalently, the states may be labeled by n_3 and the polyad number $\tilde{P} = P - 4n_3$. In this way, we obtain the ladders of states with fixed $\tilde{P}$ and n_3 in Figures 11 and 12. Within each ladder, the states are ordered according to magnitude in energy. Energy increases from the top to the bottom of the plot. A ladder $(\tilde{P},n_3)$ contains $\tilde{P}/2 + 1$ states (see eq 28). Note that in the full superpolyad these ladders overlap in a complicated way.

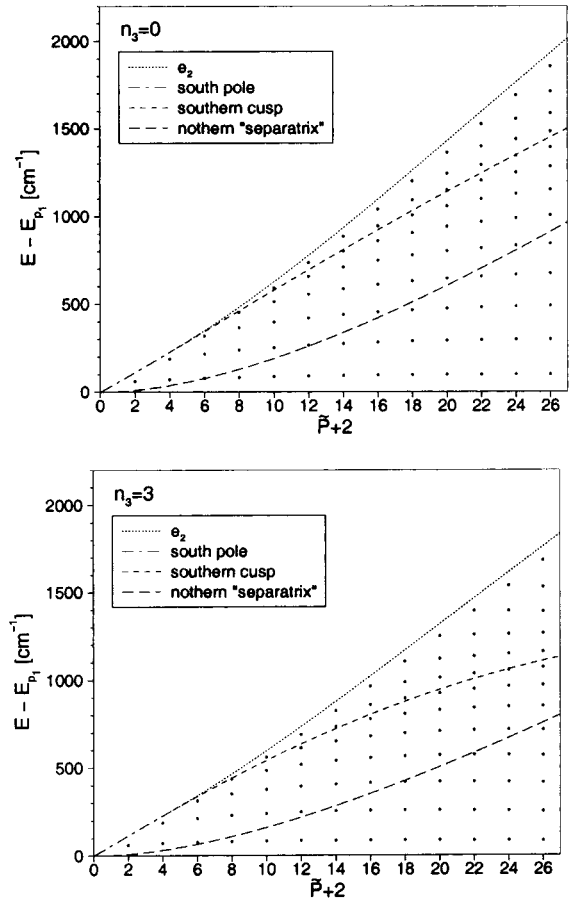

Figure 8. Location of the eigenstates (dots) relative to classical phase-space structures for different polyads $\tilde{P}$ with $n_3 = 0$ and $n_3 = 3$. The abscissa is the classical polyad $\tilde{\mathscr{P}} = \tilde{P} + 2$. The ordinate is the energy, which for reasons of graphical representation is shifted by the energy of the elliptic point e_1.

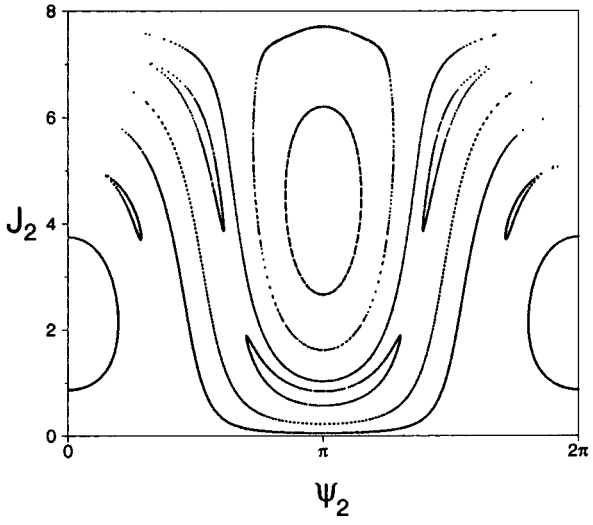

Figure 9. Superposition of Poincaré surfaces of section for superpolyad $P = 14$. The initial conditions are chosen on the quantized tori of Figure 3. In each case, the section condition is $\psi_3 = 0$ with $\dot{\psi}_3 > 0$.

Those states for which the quantum number n_3 can easily be read off, which are the great majority of the states, are expected to be located on the tori that remain of the integrable one-

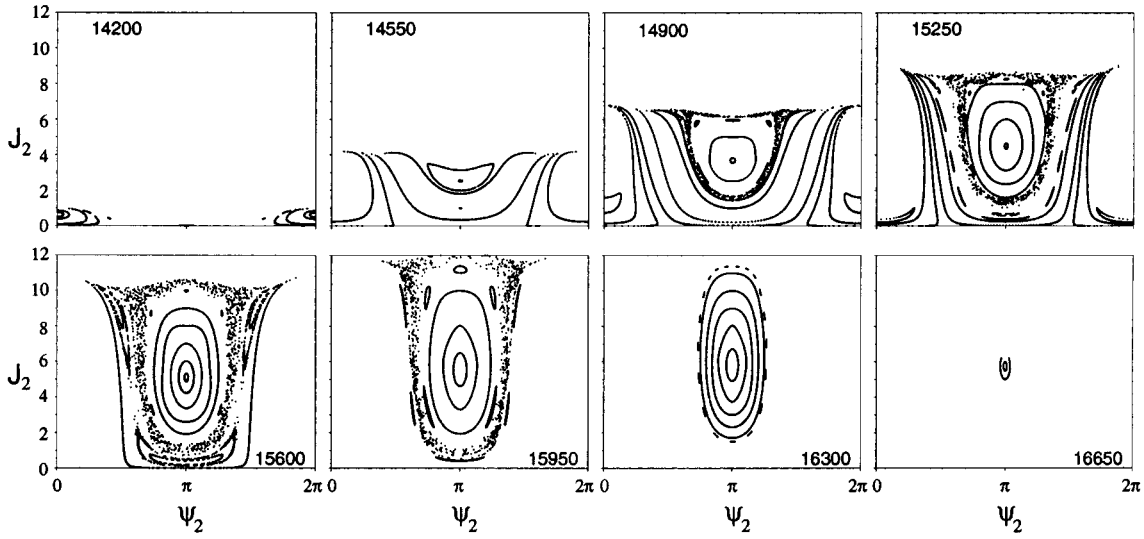

Figure 10. Poincaré surfaces of section for superpolyad $P = 22$. As in Figure 9, the section condition is again $\psi_3 = 0$ with $\dot{\psi}_3 > 0$.

resonance system after the perturbation. For these states, the location of the strip on the ψ_2 axis gives information on the type of the corresponding quantized torus. Taking into account eq 2, one concludes from the densities of states located about $\psi_2 = 0 \pmod{2\pi}$ (see the top and middle states in Figures 11 and 12) that they correspond to classical motions with $\langle \psi_2 \rangle_t = \langle \phi_1 \rangle_t - 2\langle \phi_2 \rangle_t = 0$ where $\langle ... \rangle_t$ denotes a time average. Taking the time derivative gives $\langle \dot{\psi}_2 \rangle_t = \langle \dot{\phi}_1 \rangle_t - 2\langle \dot{\phi}_2 \rangle_t = 0$, that is, an effective resonance, $\omega_1^{\text{eff}} = 2\omega_2^{\text{eff}}$, where $\omega_i^{\text{eff}} \equiv \langle \partial \mathscr{H} \partial I_i \rangle_t$ are the time-averaged effective frequencies of eq 2. By the general relation between action angle variables (I_i, ϕ_i) and the normal coordinates q_i in eq 39, the effective resonance maps to a "u" shape in the (q_1, q_2) plane. For states with densities about $\psi_2 = \pi$ (see, for example, the bottom states in Figure 12), one finds the same effective resonance, which again leads to a "u" shape, which is now reflected about the q_2 axes because of the phase shift $\langle \phi_1 \rangle_t - 2\langle \phi_2 \rangle_t = \pi$. Note that these conclusions on the classical motions may be drawn without performing any classical analysis.

For the assignment of a third quantum number to the states of a ladder with fixed $\tilde{P}$ and n_3, we look at the phase advances in the direction ψ_2. For a state with a good quantum number n_3, the expansion in eq 42 is effectively restricted to normal basis states with quantum numbers $2n_1 + n_2 = \tilde{P}$ where $\tilde{P} = P - 4n_3$. Within such a sum, n_1 runs from 0 to $\tilde{P}/2$. Accordingly, the maximum number of phase advances in units of 2π in direction ψ_2 is $\tilde{P}/2$. Obviously, the amplitudes $a_{(P,s),(n_1,n_2,n_3)}$ in eq 42 are distributed in such a way that the resulting densities of the wave functions are in accordance with the ranges of the classical motions. It is therefore natural to restrict the count of nodal lines in the direction ψ_2 to intervals with a noticeable density $|\Psi^{\text{tor}}_{(P,s)}|^2$. For states uniformly distributed about ψ_2 or localized about $\psi_2 = 0$ (see, for example, states $s = 4$ and $s = 5$ in Figure 11), this is exactly the quantum number $\tilde{n}_2$ defined in eq 33 for states that are associated with classical motions on primary tori or secondary tori about the elliptic point e_1. If we recall that the index $\tilde{s}$ labels the quantum states with increasing energy within a polyad $\tilde{P}$ with fixed n_3 and that the elliptic point e_1 corresponds to the energetic bottom of a polyad, the quantum number $\tilde{n}_2^{(e_1)}$ can be identified with $\tilde{s} - 1$. Within each ladder ($\tilde{P}$, n_3) in Figures 11 and 12, the top states correspond to $\tilde{n}_2 = 0$.

Equivalently, for states located about $\psi_2 = \pi$, the resulting quantum number is to be identified with the quantum number $\tilde{n}_2$ defined in eq 33, now for motions on secondary tori about e_2. The quantum number $\tilde{n}_2^{(e_2)}$ is equal to $\tilde{P}/2 + 1 - \tilde{s}$.

The localization of the wave functions about $\psi_2 = \pi$ at the bottom of Figures 11 and 12 increases when n_3 decreases. The localization is, for example, strongest for $n_3 = 0$ where the lines of constant phase are vertical. For the bottom states in Figure 11 with a relatively broad density about π for which the determination of the phase advances in direction ψ_2 on the range of the nonvanishing density is not so obvious, it is more convenient to count equivalently the number of valleys of the density.

The change from counting the phase advances for states localized about $\psi_2 = 0$ to counting the phase advances for states localized about $\psi_2 = \pi$ is also reflected by the discontinuity of the quantum number $\tilde{n}_2$ in Figure 5. For transient states localized close to the region of the narrow chaos band, that is, in the region of the separatrix of the one-resonance approximation, a third quantum number can be assigned by both $\tilde{n}_2^{(e_1)}$ and $\tilde{n}_2^{(e_2)}$ (see, for example, $s = 40$ in Figure 12). In particular, for large n_3, the bottom states in Figure 11 are still localized rather close to the former separatrix and they can still be assigned by $\tilde{n}_2^{(e_1)}$ (see, for example, states $s = 11$ and $s = 19$). For a ladder with a large n_3 (see, for example, the ladder ($\tilde{P}$, n_3) = (6, 4)), it is apparent that the total phase advances in units of 2π in direction ψ_2 range from 0 to $\tilde{P}/2$. In contrast to that, the assignment of the quantum number $\tilde{n}_2^{(e_1)}$ cannot be continued very far across the separatrix for ladders ($\tilde{P}$, n_3) with a small quantum number n_3 because the density almost totally vanishes away from $\psi_2 = \pi$ and the phase advances in these regions are no longer identifiable in direction ψ_2 (see, for example, states $s = 41$ and $s = 42$ in Figure 12).

By the above considerations, we were able to assign most of the states and to produce Table 2, which can be considered as the main result of this paper. For each state $|P,s\rangle$, Table 2 gives the polyad quantum number $\tilde{P} = P - 4n_3$, the approximate good quantum number n_3, and the label $\tilde{s}$, which is related to the EBK quantum number $\tilde{n}_2$ depending on whether the quantum state is localized on a primary torus, a secondary torus about e_1 or a secondary torus about e_2. The fact that, classically, the primary tori transform smoothly to the secondary tori about e_1 (see the previous section) is also reflected by the localization of the wave functions; wherefore, we do not want to overemphasize this distinction.

There are a few states that do not fit easily into this scheme. For these states, the matrix elements $\langle s,P|n_1,n_2,n_3\rangle$ with different

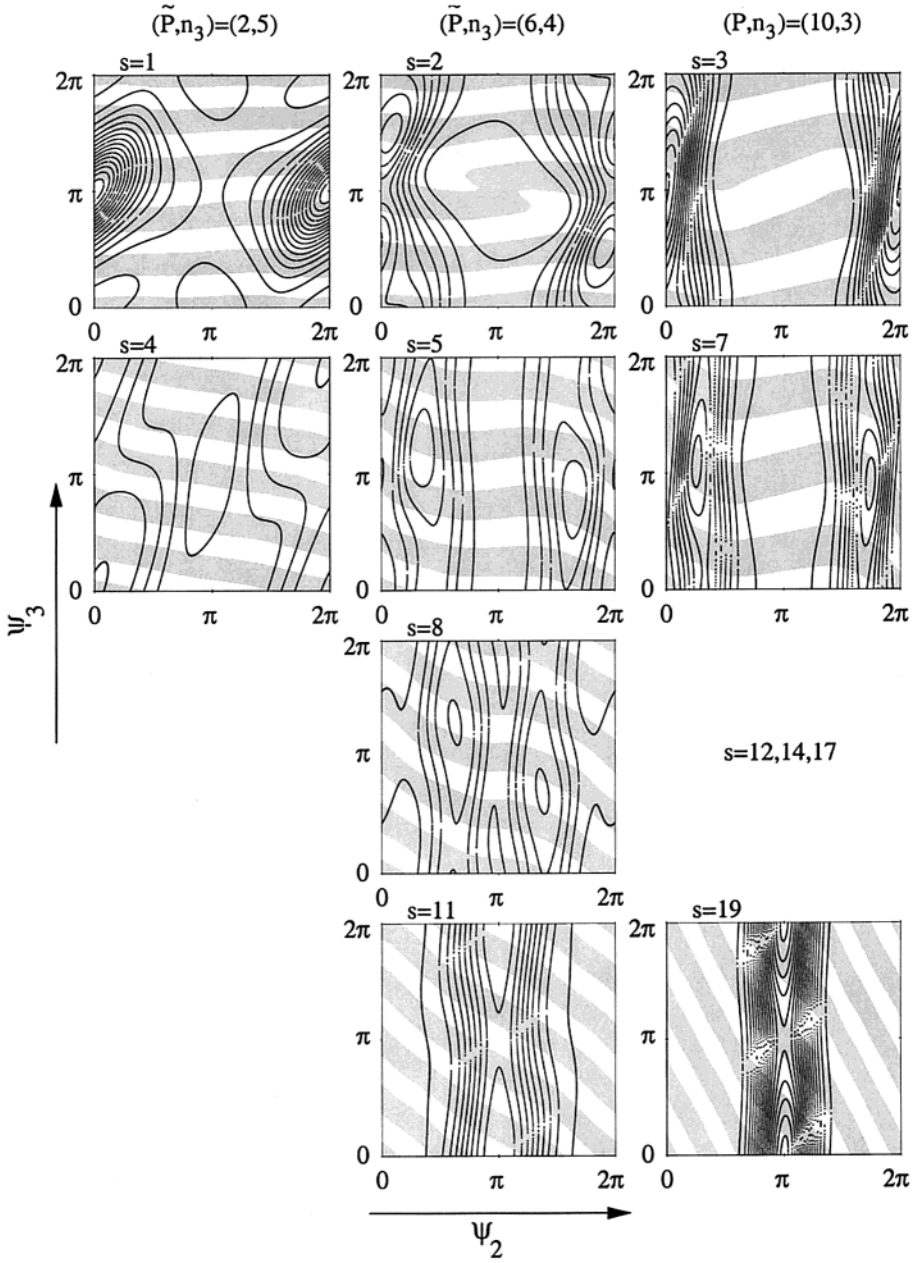

Figure 11. Densities and phases of the wave functions $\Psi^{\mathrm{tor}}_{(P,s)}$ defined in eq 40 for superpolyad $P = 22$ on the toroidal configuration space parametrized by the angles ψ_2 and ψ_3. Each column represents a ladder of constant quantum numbers $\tilde{P}$ and n_3. Within a ladder, energy increases from the top to the bottom.

n_3 noticeably mix. But having assigned most of the states that are easy to assign, there is no difficulty to include the remaining more problematic states into the assignment scheme.

With the assignment and motions in normal-mode coordinates now in hand, it is worth translating the results into internal atomic and bond motions and excitations. Clearly, n_3 tells us the degree of excitation of the decoupled asymmetric stretch. $\tilde{P}$ measures the amount of excitation energy preserved for the other degrees of freedom. The effective resonance, $\omega_1^{\mathrm{eff}} = 2\,\omega_2^{\mathrm{eff}}$, following from the vertical nature of the wave densities in Figures 11 and 12 means that the symmetric stretch variable goes through its range of values twice for one sweep of the bend variable. This can occur in two extreme ways, as at the top and bottom rows of Figures 11 and 12. Centering about $\psi_2 = 0$ corresponds to the symmetric stretch being minimally extended when the absolute value of the bend is maximal while the symmetric stretch is maximal when the bend coordinate goes to zero (see the upper left picture in Figure 6). In contrast, centering about $\psi_2 = \pi$ means that the absolute value of the bend coordinate and the symmetric stretch reach their minimum and maximum values simultaneously (see the lower right picture in Figure 6). Increasing $\tilde{s}$ represents a transition between these two extremes and is, in a sense, a measure of the dephasing from them.

Note that the simple procedure illustrated in this section almost gives all of the information obtained by different methods for the one-resonance system in the preceding section. The methods of the preceding section and their far-reaching analytical results were made possible by the neglect of all resonances up to one resonance between the symmetric stretch and the bend. For higher superpolayd numbers where the other resonances have to be included, the methods of the preceding section break down and there is almost no alternative to the procedure explained in this section.

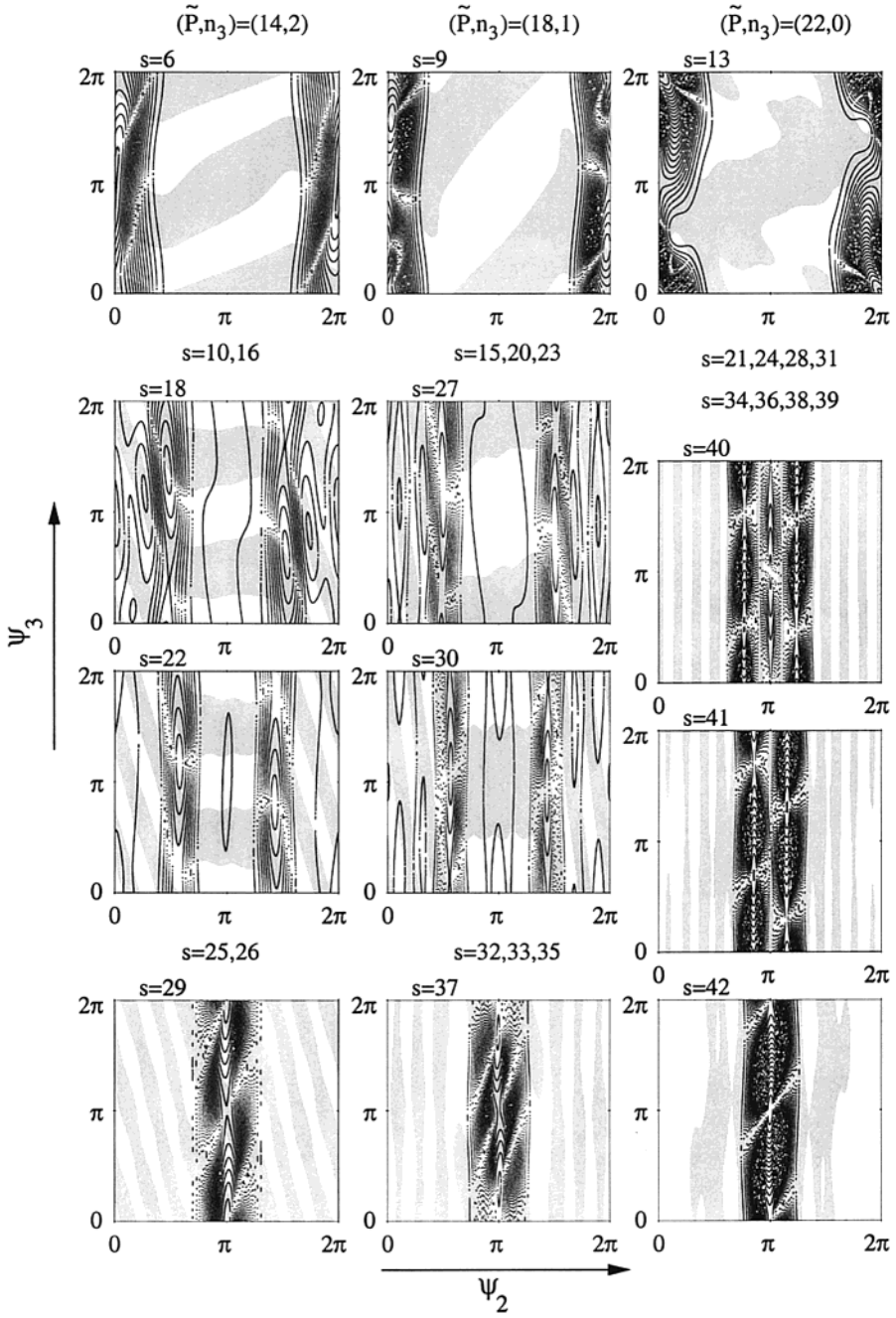

Figure 12. Continuation of Figure 11.

5. Conclusions

In this work, we represented an assignment of the vibrational spectrum of N_2O and analyzed the underlying classical motions. We showed that for low and intermediate superpolyad numbers N_2O can be well approximated by a Hamiltonian with only a single resonance between the symmetric stretch and the bend. In this approximation, the corresponding classical system is integrable and, accordingly, its phase space is foliated by invariant tori. After a change of coordinates, the two trivial degrees of freedoms, which correspond to the classical analogues of the polyad number and the quantum number of the asymmetric stretch, can be separated off and it remains a system with one effective degree of freedom of which the dynamics takes place on a so-called polyad sphere. We distinguished between the primary tori of the system without resonances and the secondary tori due to the one resonance. The centers of the secondary tori are two periodic orbits, which have a "u" shape of different orientation when projected to the space of the normal coordinates of the symmetric stretch and the bend. These periodic orbits correspond to the energetic ends of the polyads, and they appear as elliptic points on the corresponding polyad spheres. The secondary tori about the elliptic point at the energetically lower end of each polyad transform smoothly to the primary tori. In contrast to that, there is a separatrix between the secondary tori about the elliptic point at the upper ends of the polyads and the primary tori. On the polyad sphere, the separatrix maps to a cusp. The quantum states are localized on the invariant tori the actions of which fulfill EBK quantization conditions. Besides the EBK quantum numbers consisting of the polyad number $\tilde{P}$ and the separated quantum number n_3, there is one nontrivial EBK quantization to be solved. The nontrivial quantization condition can be illustrated through the

representation of the quantizing trajectories, which are the projections of the quantized tori to the polyad sphere. This representation especially gives information on which of the three types of tori the quantum mechanical wave functions are localized, which is important for the assignment in terms of EBK quantum numbers.

For higher superpolyad numbers, other resonances gain importance as was explicitly illustrated for superpolyad 22. There remains only one good quantum number, which is the superpolyad number and an analysis as for low and intermediate superpolyad numbers is no longer possible. Instead, we switched to the representation of semiclassical wave functions on the toroidal configuration space of the angle variables that remain after separating off the degree of freedom corresponding to the superpolyad number. It turned out that the classical chaos is mainly concentrated about a small band along the separatrix of the former integrable system and most of the states can still be assigned in terms of the EBK quantum number of quantized tori. The graphical representation alone already included all information on the assignment. Note that this procedure is applicable to any system for which the number of effective degrees of freedom is not greater than 2. In the application of this scheme to N_2O, the method does not display its full power because the classical dynamics is to a great extent regular and dominated by the tori of the integrable system. The scheme becomes especially interesting when classical phase space is complicated by a stronger impact of chaos and an assignment is far from obvious. The great success of the application of this procedure to acetylene[9,10] and CHBrClF[11] showed us that even for such complicated systems the classical analysis can be reduced to a minimum or might not even be necessary. Almost everything that is needed is in the graphical representation of the semiclassical wave functions on the toroidal configuration space, which are obtained with almost no further calculation. The patterns of wave functions clearly display the aspects of the classical motion, which are relevant for quantum mechanics. Some basic knowledge of action angle variables enables one to translate the relevant aspects of the motion on the configuration torus back to the motion in the original coordinates, which may be normal- or local-mode coordinates. In forthcoming papers, which will be in particular dedicated to people who are nonspecialists in the field of nonlinear dynamics, a catalog of rules for these translations will be established.

Acknowledgment. H.W. is thankful to Howard S. Taylor and the University of Southern California for hospitality during his research visit at USC in November 2000. H.S.T. acknowledges support from the U.S. National Science Foundation (Grant PHY-0071742) and the U.S. Department of Energy (Grant DE-FG03-94ER14458). In Mexico, C.J. was supported by CONACyT (Grant 33773-E).

References and Notes

(1) Teffo, J.-L.; Sulakshina, O. N.; Perevalov, V. I. *J. Mol. Spectrosc.* **1982**, *156*, 48.

(2) Teffo, J.-L.; Perevalov, V. I.; Lyulin, O. M. *J. Mol. Spectrosc.* **1994**, *168*, 390.

(3) Champargue, A.; Permogorov, D.; Bach, M.; Temsamani, M. A.; Auwera, J. V.; Herman, M.; Fujii, M. *J. Chem. Phys.* **1995**, *103*, 5931.

(4) Xiao, L.; Kellman, M. E. *J. Chem. Phys.* **1989**, *90*, 6086.

(5) Arnold, V. I. *Mathematical Methods of Classical Mechanics*; Graduate Texts in Mathematics, Vol. 60; Springer: Berlin, 1978.

(6) MacKay, R. S.; Percival, I. C.; Meiss, J. D. *Physica D* **1987**, *27*, 1.

(7) Lu, Z.-M.; Kellman, M. E. *J. Chem. Phys.* **1997**, *107*, 1.

(8) Sibert, E. L., III.; McCoy, A. B. *J. Chem. Phys.* **1986**, *105*, 469.

(9) Jacobson, M. P.; Jung, C.; Taylor, H. S.; Field, R. W. *J. Chem. Phys.* **1999**, *111*, 600.

(10) Jung, C.; Taylor, H. S.; Jacobson, M. P. *J. Phys. Chem. A* **2001**, *105*, 681.

(11) Jung, C.; Ziemniak, E.; Taylor, H. S. *J. Chem. Phys.*, submitted for publication, 2001.

(12) Joyeux, M. *J. Chem. Phys.* **1998**, *109*, 2111.

(13) McCoy, A. B.; Sibert, E. L., III Canonical Van-Vleck Perturbation Theory and its Application to Studies of Highly Vibrationally Excited States of Polyatomic Molecules. In *Dynamics of Molecules and Chemical Reactions*; Wyatt, R. E., Zhang, J. Z. H., Eds.; Dekker: New York, 1996.

(14) Fried, L.; Ezra, G. S. *J. Chem. Phys.* **1988**, *86*, 6270.

(15) Cohen-Tannoudji, C.; Diu, B.; Laloë, F. *Quantum Mechanics*; John Wiley & Sons: New York, 1997; Vol. 1.

(16) Goldstein, H. *Classical Mechanics*; Addison-Wesley: Reading, MA, 1950.

(17) Kellman, M. E. *J. Chem. Phys.* **1990**, *93*, 6630.

(18) Hose, G.; Taylor, H. S. *Phys. Rev. Lett.* **1983**, *51*, 947.

(19) Kellman, M. E.; Xiao, L. *J. Chem. Phys.* **1990**, *93*, 5821.

(20) Li, Z.; Xiao, L.; Kellman, M. E. *J. Chem. Phys.* **1990**, *92*, 2251.

(21) Xiao, L.; Kellman, M. E. *J. Chem. Phys.* **1990**, *93*, 5805.

(22) Joyeux, M.; Sugny, D.; Tyng, V.; Kellman, M. E.; Ishikawa, H.; Beck, C.; Schinke, R. *J. Chem. Phys.* **2000**, *112*, 4162.

(23) Miller, W. H. *J. Chem. Phys.* **1968**, *48*, 1651.

(24) Child, M. S. *J. Mol. Spectrosc.* **1974**, *53*, 280.

(25) Joyeux, M. *Chem. Phys.* **1997**, *221*, 287.

(26) Svitak, J.; Li, Z.; Rose, J.; Kellman, M. E. *J. Chem. Phys.* **1994**, *102*, 4340.